TISSUE ENGINEERING: Part A
Volume 22, Numbers 13 and 14, 2016

DOI: 10.1089/ten.tea.2016.0166

termis
Tissue Engineering
& Regenerative Medicine
International Society

ORIGINAL ARTICLE

Mandibular Jaw Bone Regeneration Using Human Dental Cell-Seeded Tyrosine-Derived Polycarbonate Scaffolds

Weibo Zhang, DMD, PhD,[1] Zheng Zhang, PhD,[2] Shuang Chen, PhD,[2] Lauren Macri, PhD,[2] Joachim Kohn, PhD,[2] and Pamela C. Yelick, PhD[1]

Here we present a new model for alveolar jaw bone regeneration, which uses human dental pulp cells (hDPCs) combined with tyrosine-derived polycarbonate polymer scaffolds [E1001(1k)] containing beta-tricalcium phosphate (β-TCP) [E1001(1k)/β-TCP]. E1001(1k)/β-TCP scaffolds (5 mm diameter × 1 mm thickness) were fabricated to fit a 5 mm rat mandibular ramus critical bone defect. Five experimental groups were examined in this study: (1) E1001(1k)/β-TCP scaffolds seeded with a high density of hDPCs, 5.0×10^5 hDPCs/scaffold (CH); (2) E1001(1k)/β-TCP scaffolds seeded with a lower density of hDPCs, 2.5×10^5 hDPCs/scaffold (CL); (3) acellular E1001(1k)/β-TCP scaffolds (SA); (4) acellular E1001(1k)/β-TCP scaffolds supplemented with 4 μg recombinant human bone morphogenetic protein-2 (BMP); and (5) empty defects (EDs). Replicate hDPC-seeded and acellular E1001(1k)/β-TCP scaffolds were cultured *in vitro* in osteogenic media for 1 week before implantation for 3 and 6 weeks. Live microcomputed tomography (μCT) imaging at 3 and 6 weeks postimplantation revealed robust bone regeneration in the BMP implant group. CH and CL groups exhibited similar uniformly distributed mineralized tissue coverage throughout the defects, but less than the BMP implants. In contrast, SA-treated defects exhibited sparse areas of mineralized tissue regeneration. The ED group exhibited slightly reduced defect size. Histological analyses revealed no indication of an immune response. In addition, robust expression of dentin and bone differentiation marker expression was observed in hDPC-seeded scaffolds, whereas, in contrast, BMP and SA implants exhibited only bone and not dentin differentiation marker expression. hDPCs were detected in 3-week but not in 6-week hDPC-seeded scaffold groups, indicating their survival for at least 3 weeks. Together, these results show that hDPC-seeded E1001(1k)/β-TCP scaffolds support the rapid regeneration of osteo-dentin-like mineralized jaw tissue, suggesting a promising new therapy for alveolar jaw bone repair and regeneration.

Introduction

Craniofacial defects are highly prevalent in both civilian and military populations, resulting in significant physical and psychosocial health needs.[1,2] Craniofacial alveolar jaw bones, the maxilla (upper jaw) and the mandible (lower jaw), are the ''teeth bearing'' bones, and severe injury to either is often associated with tooth fracture or loss. Current therapies to repair craniofacial jaw and tooth defects require multiple successive surgeries—first to reconstruct the alveolar bone defect and second to place dental implants after the jaw bone defect has healed[3]—requiring up to 3–6 months before full function can be restored.[4] The ability to effectively repair jaw bone and tooth defects in a coordinated manner at the same time, using combined alveolar bone and tooth constructs, could provide shorter healing times and improved outcomes.

Currently, autologous bone graft (harvested from the iliac crest, rib, tibia, or fibula) is the gold standard for craniofacial defect repair.[5] Complex maxillofacial defect repair remains quite challenging due to the limited availability of autologous bone for grafting, and the need to adapt the graft to accurately fit the defect site for optimal function and aesthetics. In addition, paraxial mesoderm-derived iliac crest bone and the long bones of the arms and legs exhibit distinctly different properties than neural crest cell (NCC)-derived craniofacial jaw bones.[6–8] The strong forces of mastication normally supported by NCC-derived alveolar jaw bone often cause the eventual resorption and failure of grafted paraxial mesoderm-derived bone, making it less desirable for applications in craniofacial bone regeneration. Regenerative approaches that avoid the need for autogenous grafts, by employing appropriate cell sources combined with

[1]Department of Orthodontics, Division of Craniofacial and Molecular Genetics, Tufts University School of Dental Medicine, Boston, Massachusetts.
[2]New Jersey Center for Biomaterials, Rutgers—The State University of New Jersey, Piscataway, New Jersey.

fabricated scaffolds and/or bioactive molecules, may provide superior alternative strategies for the effective repair of large segmental and/or composite craniofacial defects. Many types of cells, derived from both dental and nondental tissues, have been tested for craniofacial bone regeneration.[9–11] Although most cells were found to generate calcified tissues of typical bone morphology,[12–14] our prior published reports demonstrated that progenitor stem cells harvested from human dental pulp cells (hDPCs) were able to form hard tissues exhibiting characteristics of both alveolar bone and dentin.[15–17] This capability suggests that hDPCs may be promising for composite bone and tooth tissue regeneration. Here we describe the use of NCC-derived hDPCs combined with novel E1001(1k) scaffolds, as a model for superior alveolar bone regeneration strategies.

Previous publications demonstrated that cells isolated from the premature tooth buds harvested from 6-month-old discarded pig jaws retained their ability to form tooth-like structures, providing a postnatal cell source for tooth regeneration.[18] When our porcine tooth bud constructs were combined with bioengineered bone constructs, we observed the formation of tooth-alveolar bone structures.[19,20] A library of tyrosine-derived polycarbonates (TyrPCs) has been developed by combining three monomers—desaminotyrosyl-tyrosine alkyl ester (DTR; DTE when the alkyl group is an ethyl ester), desaminotyrosyl-tyrosine (DT), and poly(ethylene glycol) (PEG).[21–23] Modulation of the molar ratios of these three components within the polymer backbone allows for control of the physical, chemical, biomechanical, and biological properties of the resulting polymers.[22] To date, TyrPCs have been extensively characterized in applications as stents, drug-delivery devices, bone pins, and bone regeneration scaffolds.[24] Porous scaffolds fabricated from E1001(1k), a polymer composed of 89 mol% DTE, 10 mol% DT, and 1 mol% of a 1000 Da PEG block, were shown to support robust bone regeneration in rabbit critical sized calvarial defect and long bone defect repair models, particularly when the E1001(1k) scaffolds contained calcium phosphate.[25–27]

Based on these promising results, and on several preliminary *in vitro* studies of hDPC-seeded E1001(1k) scaffolds (data not shown), the objective of this study was to test hDPC-seeded E1001(1k)/beta-tricalcium phosphate (β-TCP) scaffolds in an alveolar bone, critical sized rat mandibular defect model.

Materials and Methods

Scaffold fabrication

Porous E1001(1k)/β-TCP scaffolds (5 mm diameter × 1 mm thickness) were fabricated as previously described.[24,25] In brief, 1.20 g of E1001(1k) (molecular weight: 270 kDa) was dissolved in 0.84 mL of deionized (DI) water and 5.16 mL of 1,4-dioxane overnight. The polymer solution was then mixed with 10.80 g of sodium chloride (NaCl) crystals (200–400 μm) and 0.51 g of β-TCP particles. The mixture was poured into a Teflon dish, quenched in liquid nitrogen, and then freeze dried. Cylindrical scaffolds were created using a 5 mm stainless steel tissue punch (Salvin Dental Specialties). NaCl was leached out with DI water, and the scaffolds were dried for 24 h in a lyophilizer. Sterilization was performed using ethylene oxide.

hDPCs isolation and implant preparation

Freshly extracted human wisdom teeth were collected following Tufts University IRB-approved protocols. Dental pulp was harvested, minced, and digested to obtain hDPCs.[28] hDPCs were expanded in dental pulp medium (DMEM/F12 with 10% FBS, 1% GlutaMAX, 50 μg/mL ascorbic acid, and 1% penicillin/streptomycin/amphotericin), and then cryopreserved. Thawed cells were then expanded and dynamically seeded onto replicate E1001(1k)/β-TCP scaffolds at two cell-seeding densities: 5.0×10^5 hDPCs/scaffold (referred to as cell high, CH), and 2.5×10^5 hDPCs/scaffold, (referred to as cell low, CL). Cell-seeded scaffolds and acellular scaffolds were cultured in dental pulp medium with osteogenic supplements (100 nM dexamethasone, 10 mM beta-glycerol phosphate, and 50 μg/mL ascorbic acid) for 1 week before *in vivo* implantation. To characterize cell penetration and attachment at the time of implantation, replicate samples ($n = 3$) were collected, sectioned, or whole mount stained with phalloidin, and imaged using an M2-Bio Zeiss fluorescent microscope (Zeiss).

Rat mandible defect surgical procedure

National Institutes of Health (NIH) guidelines for the care and use of laboratory animals (NIH Publication #85–23 Rev. 1985) have been observed. In total, 30 female nude rat hosts (RNU, Charles River, Wilmington, MA) of average weight of 300 g were used. Under isoflurane inhalation anesthesia, a full-thickness standardized defect was made using a 5 mm stainless steel tissue punch on the right mandibular ramus of individual nude rats.[29] The area was thoroughly rinsed with sterile saline to remove any remaining bone chips, and a single scaffold implant was carefully press fit into the defect. The treatment groups ($n = 6$ each) included (1) CH scaffolds, (2) CL scaffolds, (3) acellular scaffolds (SA), (4) acellular scaffolds supplemented with 4 μg recombinant human bone morphogenetic protein-2 (rhBMP2, HumanZyme, IL) (BMP), and (5) empty defects (EDs). For the BMP group, 4 μg of rhBMP-2 was added to scaffolds 30 min before implantation. Tissue layers were closed with sutures and soft gel food was provided for 3 days postsurgery.

μCT analysis

Before sample harvest, microcomputed tomography (μCT) was performed on live animals at 3 (15 rats) and 6 weeks (15 rats) postimplantation using a SkyScan 1176 μCT (SkyScan/Bruker Micro-CT) and a 0.5 mm aluminum filter with a resolution of 9 μm. The resulting cross-sectional images were postprocessed by NRecon (Bruker). The volume of newly formed hard tissue within the defect area of each sample was evaluated using image analysis software Avizo9.0 (FEI) with the threshold of 70–255.

Construct harvest, histological, and immunohistochemical analyses

After μCT, rat hosts were euthanized using carbon dioxide gas inhalation. Mandibles were harvested, fixed in 10% formalin, treated with 30% sucrose, and embedded in optimal cutting temperature compound for frozen sectioning. To preserve the morphology of sectioned specimens, 10 μm coronal

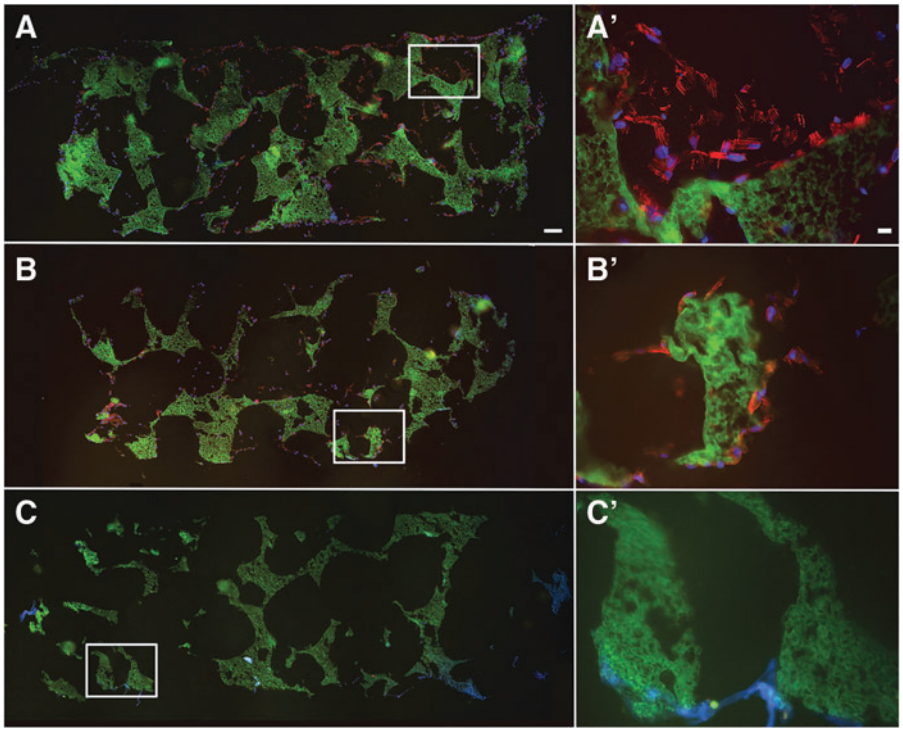

FIG. 1. hDPC-seeded E1001(1k)/β-TCP scaffolds. hDPC-seeded and acellular scaffolds were cultured in osteogenic media for 1 week before implantation. Cytoskeletal F-Actin was stained using Alexa Fluor 594-conjugated phalloidin (*red*). Nuclei were stained with Hoechst 33258 (*blue*). E1001(1k)/β-TCP scaffolds exhibited autofluorescence under GFP filter (*green*). **(A)** Scaffold seeded with high cell density. **(B)** Scaffold seeded with low cell density. **(C)** Acellular scaffold. **(A′–C′)** show high magnification of corresponding *boxed areas*. Scale bars = 500 μm **(A–C)** and 20 μm **(A′–C′)**. hDPC, human dental pulp cell. Color images available online at www.liebertpub.com/tea

serial sections were prepared using tape (Cryofilm Type2C; Section-Lab) to transfer sections to microscope slides.

Unstained sections were first imaged by fluorescent microscopy using the 4′,6-diamidino-2-phenylindole (DAPI) filter on a Zeiss Axiophot microscope and digital Zeiss Axiocam camera (Carl Zeiss AG) to identify remaining scaffold at the defect site, which fluoresced blue under these conditions. Von Kossa stain was then used to identify and quantify mineralized tissue formation in each sample. Overlay of fluorescent and von Kossa stained images was used to identify newly formed mineralized tissue within each defect. Selected sections were decalcified and stained with Gemori trichrome stain (HT10316; Sigma-Aldrich). Green fluorescent protein fluorescent residual E1001(1k)/β-TCP scaffold (green) was easily distinguishable from Gemori-stained regenerated bone (blue) and soft tissues (brown). Immunofluorescent analyses were performed using the following antibodies: antiosteocalcin (OC, ab13418; Abcam), antidentin sialophosphoprotein

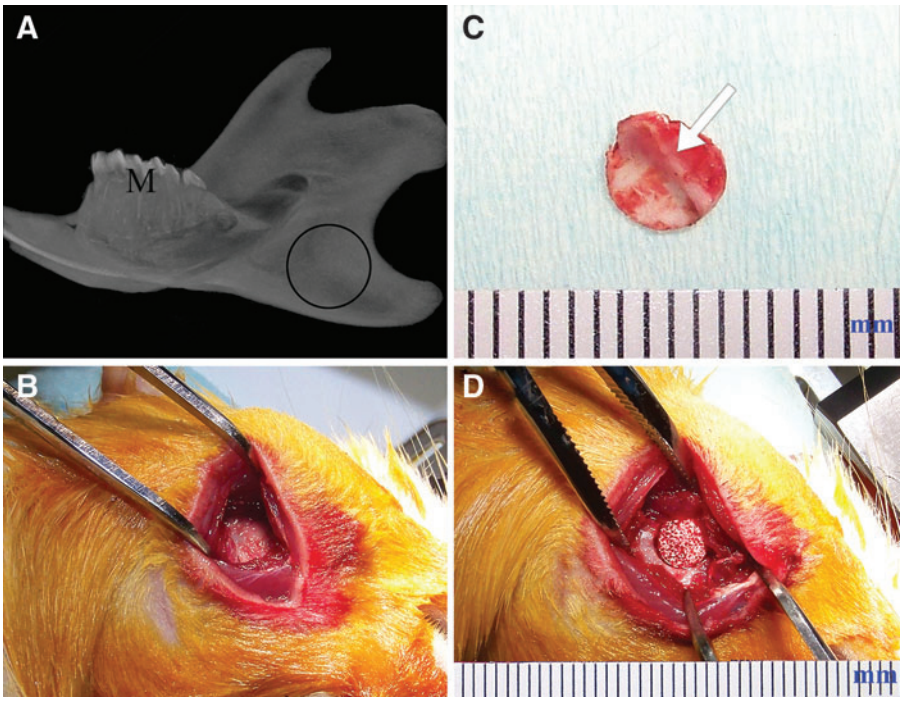

FIG. 2. Rat mandibular defect model. **(A)** Schematic diagram of the 5 mm in diameter, full thickness, circular defect in the rat mandible. **(B)** Exposed operation site. **(C)** A piece of punch out full thickness bone chip. Bone surface bridge-like structure can be clearly seen (*arrow*). **(D)** E1001(1k)/β-TCP scaffold can be tightly fit into the bone defect. M, molar. Scale bar: The units on the ruler indicate millimeters. Color images available online at www.liebertpub.com/tea

(DSPP, GTX60194; GeneTex), and antihuman mitochondria (ab122321; Abcam).

Statistical analyses

All data were presented as mean ± SD. Statistical significance values were defined as $p \leq 0.05$ based on one-way analysis of variance comparing data from every two experimental groups, which were analyzed using Microsoft Excel software.

Results

hDPCs exhibited uniform distribution in E1001(1k)/β-TCP scaffolds

E1001(1k)/β-TCP scaffolds exhibited a bimodal pore-size distribution of interconnected macropores (diameter about 200–400 μm) and micropores (diameter < 20 μm), as previously published.[24] Alizarin red staining demonstrated an even distribution of calcium phosphate throughout the scaffold (Supplementary Fig. S1; Supplementary Data are available online at www.liebertpub.com/tea). hDPCs, seeded onto scaffolds and cultured *in vitro* for 1 week, exhibited a typical mesenchymal cell morphology (Fig. 1A). Phalloidin staining demonstrated that both CH and CL scaffolds exhibited healthy multilayered cells present on the surface and throughout the scaffolds (Fig. 1A, A′, B, B′) and demonstrated an even hDPC distribution throughout cell-seeded scaffolds before implantation.

Mandibular defect surgery

The right mandibular ramus was selected as the implant site, whereas the left side served as an unoperated control (Fig. 2A). Clean, full thickness 5 mm defects were created (Fig. 2B). The anatomically distinct boney ridge of the ramus was clearly observed on the lingual side of each alveolar bone punch (Fig. 2C, arrow). hDPC-seeded and acellular scaffolds were press fitted into the 5-mm punched mandibular defect (Fig. 2D). All skin wounds healed within 7 days, and no obvious weight loss was observed in any of the host animals. None of the host animals exhibited any adverse reactions, indicative of implant biocompatibility.

μCT analyses

μCT analyses revealed an identifiable radiolucent circular defect site in the right mandibular ramus of each operated animal at 3 and 6 weeks (Fig. 3A). Small radiopaque areas were observed in the defect region of all of the CH, CL, and SA replicate samples, indicating new mineralized tissue formation (Fig. 3A). Both CH and CL groups exhibited more uniformly distributed calcified tissue formation throughout

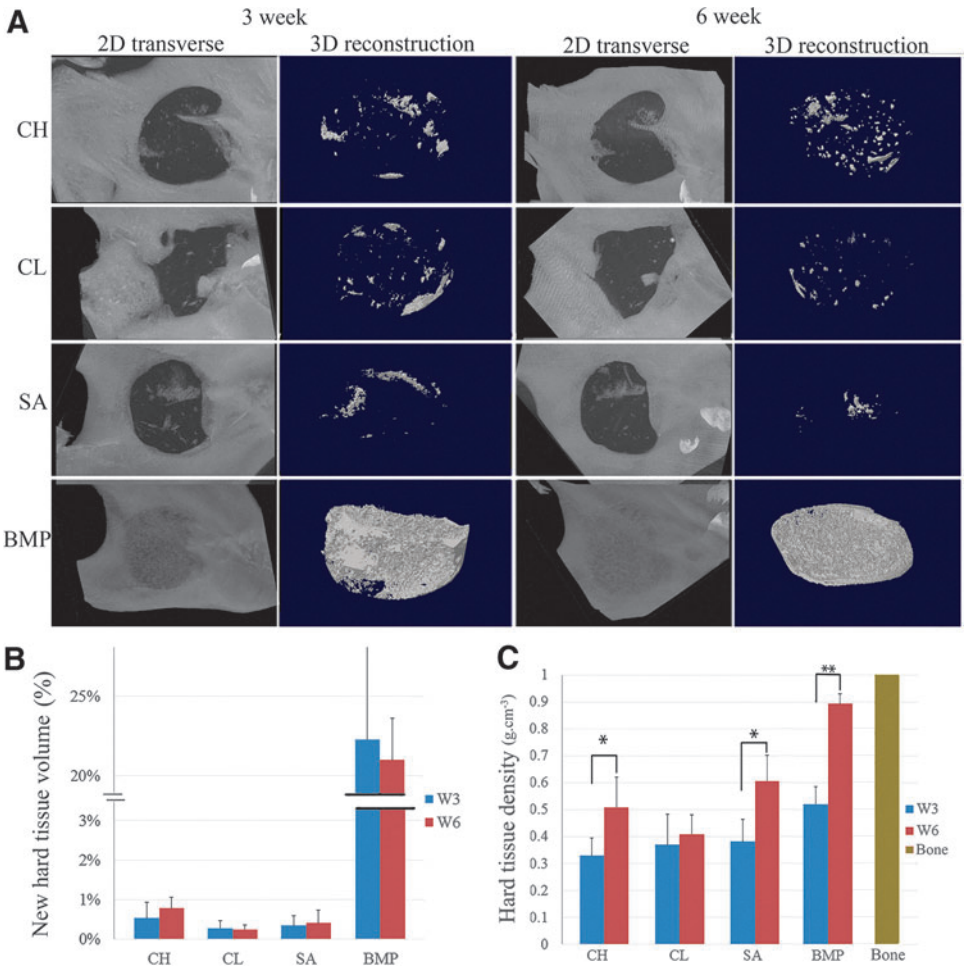

FIG. 3. μCT analysis. **(A)** Representative μCT images of mineralized tissue formation in rat mandibular defects at 3 and 6 weeks post-implantation. **(B)** New hard tissue volume (%) within each scaffold was quantified using μCT image analyses. Data are reported as a mean ± standard deviation. Statistically different mineralized tissue volume formation was found between the BMP-loaded scaffolds and the other experimental conditions at the same time period ($p < 0.01$). **(C)** Average hard tissue density within each scaffold was quantified using μCT image analyses. Significant differences were found in hard tissue density between the 3-week and 6-week of CH implants ($P < 0.05$), SA implants ($P < 0.05$) and BMP implants ($P < 0.01$). BMP, bone morphogenetic protein; uCT, microcomputed tomography. Color images available online at www.liebertpub.com/tea

the scaffold than the unseeded SA samples. BMP-loaded scaffold defects exhibited dense calcified tissue formation, with only a faint border detectable with the surrounding native mandibular bone (Fig. 3A). Three-dimensional (3D) modeling of the μCT images revealed the regeneration of an alveolar boney ridge structure in BMP-loaded scaffolds and to a limited extent in hDPC-seeded and acellular E1001(1k)/β-TCP scaffold implants, which resembled the natural boney ridge present in the biopunched mandible (Fig. 3A). Statistical analyses demonstrated significantly increased hard tissue densities and volume in BMP scaffolds as compared with all other implants ($p < 0.05$; Fig. 3B, C). Significant differences were found in hard tissue density formation between the 3 weeks and 6 weeks of CH implants ($p < 0.05$), SA implants ($p < 0.05$), and BMP implants ($p < 0.01$), but not in between CH, CL, and SA groups. CH scaffold defects trended higher mineralized tissue volume than the CL and SA groups (Fig. 3B).

The average critical sized defect reduced to 2.9 mm in diameter after 3 weeks, and 2.5 mm in diameter after 6 weeks, indicating some healing of the original 5.0 mm defect (Supplementary Fig. S2). Comparison of SA and ED groups

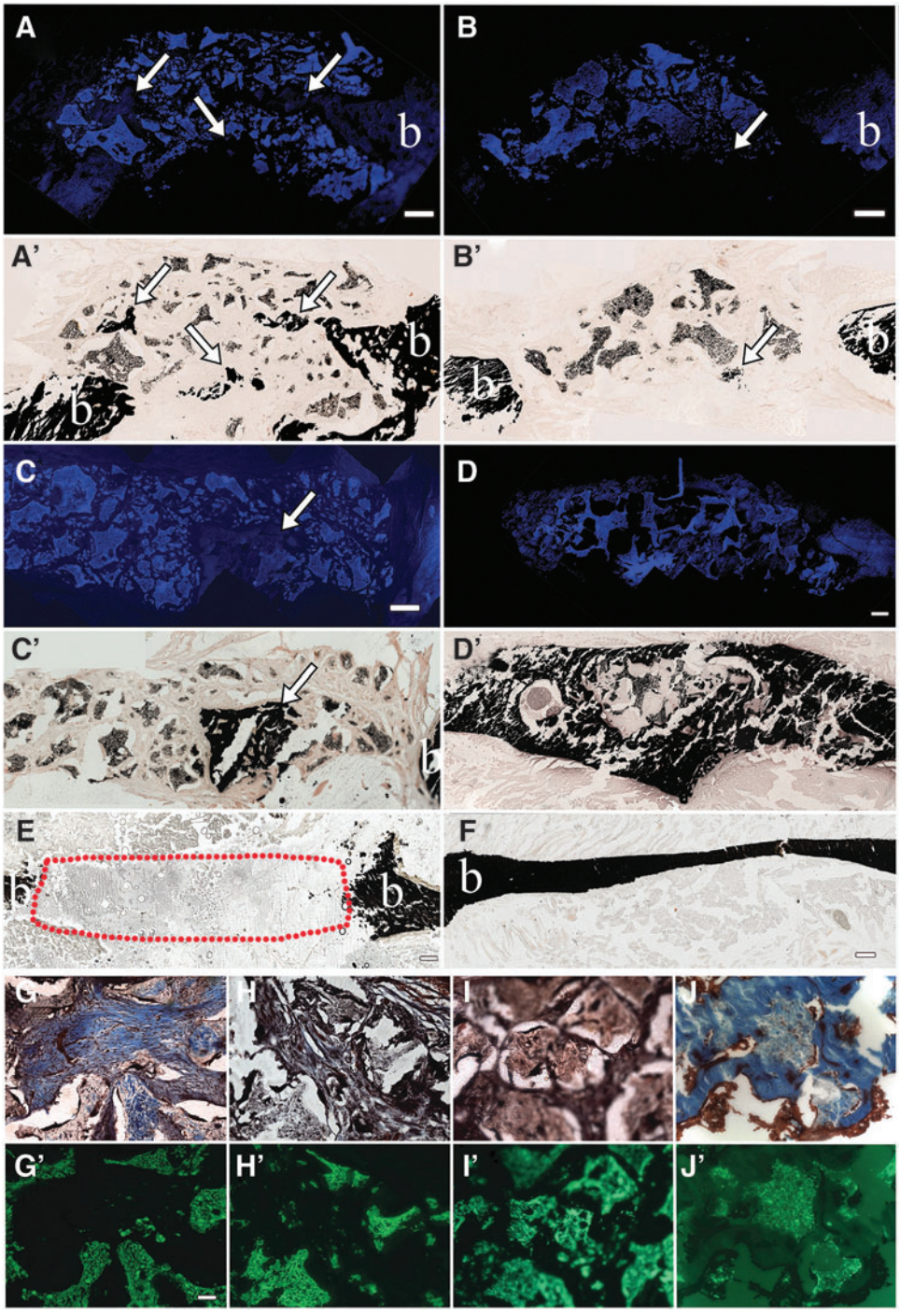

FIG. 4. Histological analysis of mandibular bone defect healing. Coronal sectioned rat mandible defects at 6 weeks postimplantation. **(A–D)** E1001(1k) scaffolds exhibit *blue* autofluorescence under DAPI filter. **(A′–D′)** Identical sections stained with von Kossa show *black* staining of mineralized tissue formation within the scaffolds (*white arrows*). **(E)** ED. **(F)** Natural bone control. **(G–J)** Gemori trichrome-stained specimens show new bone formation stained *blue*, and soft tissue stained *brown* under bright field microscopy. **(G′–J′)** Identical sections viewed under GFP fluorescence show E1001(1k) scaffold autofluorescence in *green*. Scale bar = 500 μm **(A–F)**, and 50 μm **(G–J, G′–J′)**. BMP, bone morphogenetic protein; CH, high cell-seeding density; CL, low cell-seeding density; SA, scaffold alone. ED, empty defect; SA, scaffolds. Color images available online at www.liebertpub.com/tea

indicated some inhibition of new bone in-growth into the acellular E1001(1k)/β-TCP scaffold at 3 and 6 weeks.

Histological analyses of regenerated hard and soft tissue formation

Histological analyses were used to characterize mineralized and soft tissue formation in all samples. Mineralized tissue formation was assessed using von Kossa stain, which was found to stain the E1001(1k)/β-TCP scaffold itself. We, therefore, used fluorescent microscopy with a DAPI filter to distinguish the autofluorescence of the scaffold from the nonfluorescent newly formed mineralized tissue. Similar to our μCT results, we found that small areas of newly formed calcified tissue were detected throughout the hDPC-seeded scaffolds, whereas only a fewer but larger areas of hard tissue were present in unseeded SA defect sites (Fig. 4 A–C, A′–C′).

As already described, E1001(1k)/β-TCP scaffolds regenerated the boney ridge observed in the natural rat mandible (Fig. 4D, D′ and Supplementary Video S1), suggesting the ability to respond to unique mechanical forces and surrounding craniofacial skeletal geometries for alveolar bone regeneration. At both 3 and 6 weeks, regenerated BMP-loaded E1001(1k)/β-TCP scaffold-derived bone showed no detectable margin between the implant and surrounding native bone. In comparison, EDs were not fully healed even after 6 weeks (Fig. 4E, red dotted area). Gemori trichrome staining revealed that all scaffold-containing defects exhibited close integration with the surrounding native tissues at 3 and 6 weeks, indicative of a tight fit with no dislocations (Fig. 4G–J, G′–J′). Especially in areas of significant hard tissue formation, it was difficult to distinguish the scaffold material from the newly formed hard tissue (Fig. 4G, J, G′, J′). No obvious lymphocytic infiltrates were observed in any of the samples.

To correlate with CT and histological analyses, hard tissue formation was further characterized by IF staining for the bone marker OC.[30,31] and the alveolar bone and dentin marker DSPP.[32,33] OC expression was detected in all scaffolds consistent with new mineralized tissue formation (Fig. 5A). In contrast, the odontoblast/alveolar bone differentiation marker DSPP was only detected in hDPSC-seeded scaffold implants, and not in the SA- or BMP-loaded samples (Fig. 5B). These results indicate the formation of osteodentin-like tissue by the hDPCs, which expressed both OC and DSPP. The presence of hDPCs within cell-seeded scaffolds was detected at 3 weeks postimplantation using the human mitochondria antibody (Fig. 5C, arrows), but not in 6-week implants.

Discussion

Over the past few decades, remarkable progress has been made in the development of improved surgical techniques and clinical outcomes for craniofacial defect repair. Despite this progress, craniofacial bone regeneration remains a significant clinical challenge, partly due to insufficient detailed knowledge and understanding of molecular factors regulating bone regeneration.[34] Based on successful bone regeneration therapies, biomimetic bone graft substitutes should exhibit high biocompatibility, support cell attachment, proliferation, and direct the formation of extracellular matrix throughout the defect, which can be rapidly mineralized.[35,36] Furthermore, ideal bone substitutes should exhibit mechanical properties

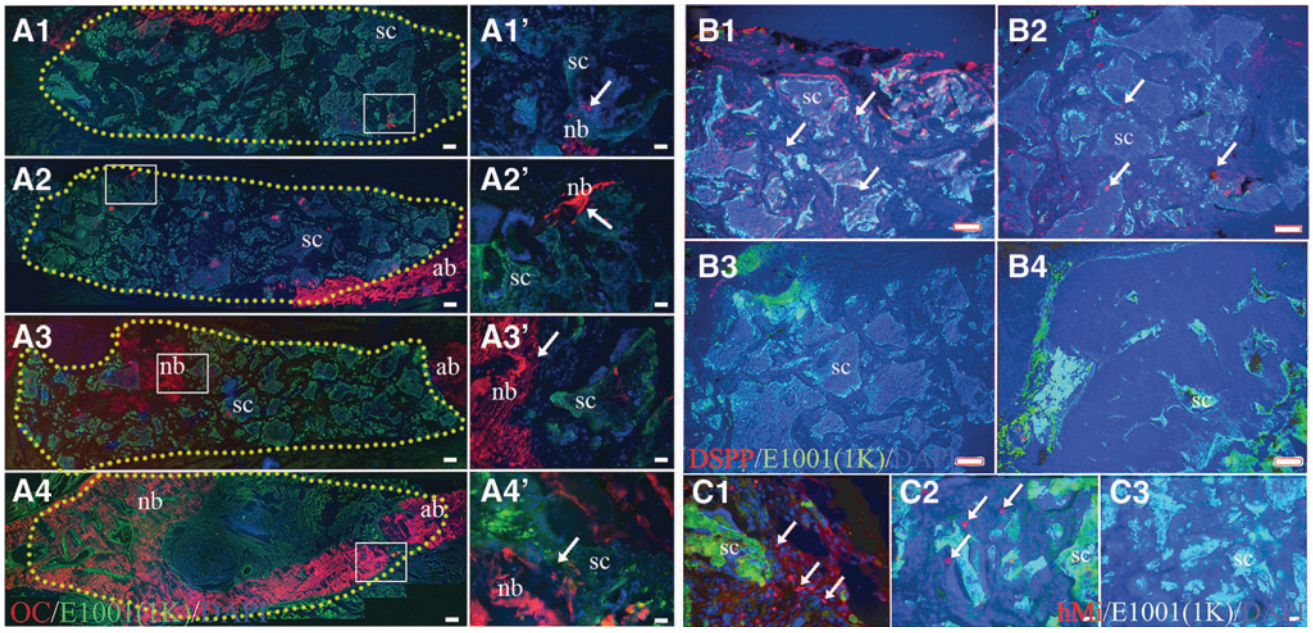

FIG. 5. Immunofluorescent analyses of rat mandibular defect healing. Positive immunostaining is indicated in *red*, E1001(1k)-bTCP scaffold autofluorescence in *green*. **(A)** OC staining. **(A1′–A4′)** Higher magnification images of the correlated *boxed area* of **(A1–A4)**. **(A1, A1′)** Cell-high density-6W; **(A2, A2′)** cell-low density-6W; **(A3, A3′)** scaffold alone-6W; **(A4, A4′)** BMP-6W; *yellow dots* outline the border of scaffolding area. **(B)** DSPP staining; **(B1)** cell-high density-6W; **(B2)** cell-low density-6W; **(B3)** scaffold alone-6W; **(B4)** BMP-6W. **(C)** Human mitochondria staining; **(C1)** cell-high density-3W; **(C2)** cell-low density-3W; **(C3)** scaffold alone-3W. Scale bar = 500 μm **(A1–A4)**, 50 μm **(B1–B4)**, 20 μm **(A1′–A4′, C1–C3)**. DSPP, dentin sialophosphoprotein; SC, scaffold; nb, normal bone. Color images available online at www.liebertpub.com/tea

that support and maintain craniofacial structure and function during the bone healing process, and be easily and accurately shaped to fit the uniquely complex craniofacial anatomies.[37,38]

A variety of materials have been analyzed for use in craniofacial reconstructions, including titanium,[39] calcium phosphate,[40,41] and synthetic polymer scaffolds.[42] These reports showed that 3D biomimetic scaffolds exhibiting physical properties that closely resembled the target tissue provided the best outcomes for tissue regeneration. Therefore, scaffolds that mimic the physiological Haversian systems present in natural bone, which have an approximate diameter of 100 μm, may be most suitable for bone regeneration.[43]

The porous E1001(1k)/β-TCP scaffolds used in this study were created to exhibit an interconnected bimodal pore structure, including macropores of 200–400 μm in diameter to facilitate cellular infiltration and induce bone formation, and also micropores of less than 20 μm in diameter to promote diffusion of oxygen and nutrients, and the formation of bone-like apatite formation.[44] In this study, we observed mineralized tissue regeneration within and on the surface of both hDPC-seeded and acellular scaffolds, further supporting the osteoconductivity of these scaffolds. In addition, the presence of new bone formation in acellular scaffold implants indicates the ability of E1001(1k)/β-TCP scaffolds to recruit host cell participation in mineralized tissue regeneration.

μCT and histological analyses showed that defects implanted with hDPC-seeded E1001(1k)/β-TCP scaffolds exhibited a unique pattern of mineralized tissue formation as compared with acellular scaffolds. Fewer but larger calcified tissue fragments were observed within acellular scaffold defects, whereas broader areas of smaller, evenly distributed bone fragments were regenerated within the hDPC-seeded scaffold. Furthermore, the expression of DSPP, a dentin-specific matrix protein normally expressed in naturally formed alveolar bone, was only observed in hDPC-seeded scaffold-derived regenerated bone, and not in BMP-loaded or acellular scaffolds. These results suggest that E1001(1k)/β-TCP scaffolds exhibit the ability to support hDPC differentiation into dentin-producing odontoblasts, and to form mineralized alveolar bone tissue resembling natural jaw bone. We further demonstrated that hDPCs are present in CH and CL scaffolds at 3 weeks, but not at 6 weeks. These results are consistent with numerous reports showing lack of long-term survival of human cells after implantation, while still contributing to target tissue regeneration.[45]

The osteoinductive factor BMP-2 has been evaluated for treatment of large-sized boney defects in a variety of animal models,[46,47] and has received Food and Drug Administration (FDA) approval for use in challenging cases of bone regeneration in humans,[48] including the repair of critical sized craniofacial defects.[49,50] It was previously shown that E1001(1k) scaffolds can be used for the controlled delivery and release of growth factors including rhBMP-2.[25] In this study, rhBMP-2-loaded E1001(1k)/β-TCP scaffolds promoted robust calcified tissue formation in a rat mandibular defect model, suggesting therapeutic uses for alveolar bone formation. The complete regeneration of the alveolar jaw bone defect, including the physiologically distinct boney surface ridge structure, further validates this model. Several reports of a critical sized rat mandible defect showed that defects greater than or equal to 4.0 mm in diameter failed to heal spontaneously within 24 weeks.[51–53] In our study, we found a significant decrease in the diameter of our ED control at both 3 and 6 weeks (Supplementary Fig. S3). For this reason, we were very careful to restrict our measurement of new bone formation within the scaffolding region alone.

Conclusions

In summary, we have shown that E1001(1k)/β-TCP scaffolds exhibit physical properties similar to natural bone, support the regeneration of hDPC-derived alveolar bone-like calcified tissue, and provide a promising synthetic bone graft substitute for use in alveolar bone regeneration. In the future, with the help of medical imaging and computational modeling techniques, E1001(1k)/β-TCP scaffolds can be easily prefabricated and shaped to fit patient-specific craniofacial defects.

Acknowledgments

This study was supported by DoD/AFIRM II Award #W81XWH-14–2-0004 (PCY), NIH/NIDCR R01 DE016132 (PCY), by Award Number P41EB001046 from the National Institute of Biomedical Imaging and Bioengineering, and discretionary funds from the New Jersey Center for Biomaterials at Rutgers University. The content is solely the responsibility of the authors and does not necessarily represent the official views of the National Institute of Biomedical Imaging and Bioengineering or the National Institutes of Health.

Disclosure Statement

No competing financial interests exist.

References

1. Davis, R.E., and Telischi, F.F. Traumatic facial nerve injuries: review of diagnosis and treatment. J Craniomaxillofac Trauma **1,** 30, 1995.
2. Curtis, D.A., Plesh, O., Miller, A.J., Curtis, T.A., Sharma, A., Schweitzer, R., Hilsinger, R.L., Schour, L., and Singer, M. A comparison of masticatory function in patients with or without reconstruction of the mandible. Head Neck **19,** 287, 1997.
3. Laine, J., Vahatalo, K., Peltola, J., Tammisalo, T., and Happonen, R.P. Rehabilitation of patients with congenital unrepaired cleft palate defects using free iliac crest bone grafts and dental implants. Int J Oral Maxillofac Implants **17,** 573, 2002.
4. Coulthard, P., Esposito, M., Jokstad, A., and Worthington, H.V. Interventions for replacing missing teeth: bone augmentation techniques for dental implant treatment. Cochrane Database Syst Rev, CD003607, 2003.
5. Dimitriou, R., Jones, E., McGonagle, D., and Giannoudis, P.V. Bone regeneration: current concepts and future directions. BMC Med **9,** 66, 2011.
6. Oppenheimer, A.J., Tong, L., and Buchman, S.R. Craniofacial bone grafting: Wolff's law revisited. Craniomaxillofac Trauma Reconstr **1,** 49, 2008.
7. Chai, Y., and Maxson, R.E., Jr. Recent advances in craniofacial morphogenesis. Dev Dyn **235,** 2353, 2006.
8. Aghaloo, T.L., Chaichanasakul, T., Bezouglaia, O., Kang, B., Franco, R., Dry, S.M., Atti, E., and Tetradis, S. Osteogenic potential of mandibular vs. long-bone marrow stromal cells. J Dent Res **89,** 1293, 2010.

9. Pagni, G., Kaigler, D., Rasperini, G., Avila-Ortiz, G., Bartel, R., and Giannobile, W.V. Bone repair cells for craniofacial regeneration. Adv Drug Deliv Rev **64,** 1310, 2012.
10. Kaigler, D., Pagni, G., Park, C.H., Tarle, S.A., Bartel, R.L., and Giannobile, W.V. Angiogenic and osteogenic potential of bone repair cells for craniofacial regeneration. Tissue Eng Part A **16,** 2809, 2010.
11. Robey, P.G., Kuznetsov, S.A., Ren, J., Klein, H.G., Sabatino, M., and Stroncek, D.F. Generation of clinical grade human bone marrow stromal cells for use in bone regeneration. Bone **70,** 87, 2015.
12. Soltan, M., Smiler, D., Prasad, H.S., and Rohrer, M.D. Bone block allograft impregnated with bone marrow aspirate. Implant Dent **16,** 329, 2007.
13. Tobita, M., Uysal, A.C., Ogawa, R., Hyakusoku, H., and Mizuno, H. Periodontal tissue regeneration with adipose-derived stem cells. Tissue Eng Part A **14,** 945, 2008.
14. Jin, Q.M., Anusaksathien, O., Webb, S.A., Rutherford, R.B., and Giannobile, W.V. Gene therapy of bone morphogenetic protein for periodontal tissue engineering. J Periodontol **74,** 202, 2003.
15. Iohara, K., Zheng, L., Ito, M., Tomokiyo, A., Matsushita, K., and Nakashima, M. Side population cells isolated from porcine dental pulp tissue with self-renewal and multipotency for dentinogenesis, chondrogenesis, adipogenesis, and neurogenesis. Stem Cells **24,** 2493, 2006.
16. Zhang, W., Walboomers, X.F., van Kuppevelt, T.H., Daamen, W.F., Bian, Z., and Jansen, J.A. The performance of human dental pulp stem cells on different three-dimensional scaffold materials. Biomaterials **27,** 5658, 2006.
17. Zhang, W., Walboomers, X.F., van Osch, G.J., van den Dolder, J., and Jansen, J.A. Hard tissue formation in a porous HA/TCP ceramic scaffold loaded with stromal cells derived from dental pulp and bone marrow. Tissue Eng Part A **14,** 285, 2008.
18. Young, C.S., Terada, S., Vacanti, J.P., Honda, M., Bartlett, J.D., and Yelick, P.C. Tissue engineering of complex tooth structures on biodegradable polymer scaffolds. J Dent Res **81,** 695, 2002.
19. Abukawa, H., Zhang, W., Young, C.S., Asrican, R., Vacanti, J.P., Kaban, L.B., Troulis, M.J., and Yelick, P.C. Reconstructing mandibular defects using autologous tissue-engineered tooth and bone constructs. J Oral Maxillofac Surg **67,** 335, 2009.
20. Zhang, W., Abukawa, H., Troulis, M.J., Kaban, L.B., Vacanti, J.P., and Yelick, P.C. Tissue engineered hybrid tooth-bone constructs. Methods **47,** 122, 2009.
21. Bourke, S.L., and Kohn, J. Polymers derived from the amino acid L-tyrosine: polycarbonates, polyarylates and copolymers with poly(ethylene glycol). Adv Drug Deliv Rev **55,** 447, 2003.
22. Pulapura, S., and Kohn, J. Tyrosine-derived polycarbonates: backbone-modified ''pseudo''-poly (amino acids) designed for biomedical applications. Biopolymers **32,** 411, 1992.
23. Magno, M.H.R., Kim, J., Srinivasan, A., McBride, S., Bolikal, D., Darr, A., Hollinger, J.O., and Kohn, J. Synthesis, degradation and biocompatibility of tyrosine-derived polycarbonate scaffolds. J Mater Chem **20,** 8885, 2010.
24. Kim, J., Magno, M.H., Alvarez, P., Darr, A., Kohn, J., and Hollinger, J.O. Osteogenic differentiation of pre-osteoblasts on biomimetic tyrosine-derived polycarbonate scaffolds. Biomacromolecules **12,** 3520, 2011.
25. Kim, J., Magno, M.H., Waters, H., Doll, B.A., McBride, S., Alvarez, P., Darr, A., Vasanji, A., Kohn, J., and Hollinger, J.O. Bone regeneration in a rabbit critical-sized calvarial model using tyrosine-derived polycarbonate scaffolds. Tissue Eng Part A **18,** 1132, 2012.
26. Guda, T., Darr, A., Silliman, D.T., Magno, M.H., Wenke, J.C., Kohn, J., and Brown Baer, P.R. Methods to analyze bone regenerative response to different rhBMP-2 doses in rabbit craniofacial defects. Tissue Eng Part C Methods **20,** 749, 2014.
27. Kim, J., McBride, S., Donovan, A., Darr, A., Magno, M.H., and Hollinger, J.O. Tyrosine-derived polycarbonate scaffolds for bone regeneration in a rabbit radius critical-size defect model. Biomed Mater **10,** 035001, 2015.
28. Zhang, W., Ahluwalia, I.P., Literman, R., Kaplan, D.L., and Yelick, P.C. Human dental pulp progenitor cell behavior on aqueous and hexafluoroisopropanol based silk scaffolds. J Biomed Mater Res A **97,** 414, 2011.
29. Kaban, L.B., and Glowacki, J. Induced osteogenesis in the repair of experimental mandibular defects in rats. J Dent Res **60,** 1356, 1981.
30. Xiao, Y., Haase, H., Young, W.G., and Bartold, P.M. Development and transplantation of a mineralized matrix formed by osteoblasts in vitro for bone regeneration. Cell Transplant **13,** 15, 2004.
31. Malicev, E., Marolt, D., Kregar Velikonja, N., Kreft, M.E., Drobnic, M., and Rode, M. Growth and differentiation of alveolar bone cells in tissue-engineered constructs and monolayer cultures. Biotechnol Bioeng **100,** 773, 2008.
32. Chen, S., Gluhak-Heinrich, J., Wang, Y.H., Wu, Y.M., Chuang, H.H., Chen, L., Yuan, G.H., Dong, J., Gay, I., and MacDougall, M. Runx2, osx, and dspp in tooth development. J Dent Res **88,** 904, 2009.
33. Chen, Y., Zhang, Y., Ramachandran, A., and George, A. DSPP is essential for normal development of the dental-craniofacial complex. J Dent Res **95,** 302, 2016.
34. Amini, A.R., Laurencin, C.T., and Nukavarapu, S.P. Bone tissue engineering: recent advances and challenges. Crit Rev Biomed Eng **40,** 363, 2012.
35. Groeneveld, E.H., van den Bergh, J.P., Holzmann, P., ten Bruggenkate, C.M., Tuinzing, D.B., and Burger, E.H. Mineralization processes in demineralized bone matrix grafts in human maxillary sinus floor elevations. J Biomed Mater Res **48,** 393, 1999.
36. Yang, S., Leong, K.F., Du, Z., and Chua, C.K. The design of scaffolds for use in tissue engineering. Part I. Traditional factors. Tissue Eng **7,** 679, 2001.
37. Popov, V.K., Evseev, A.V., Ivanov, A.L., Roginski, V.V., Volozhin, A.I., and Howdle, S.M. Laser stereolithography and supercritical fluid processing for custom-designed implant fabrication. J Mater Sci Mater Med **15,** 123, 2004.
38. Antonov, E.N., Bagratashvili, V.N., Whitaker, M.J., Barry, J.J., Shakesheff, K.M., Konovalov, A.N., Popov, V.K., and Howdle, S.M. Three-dimensional bioactive and biodegradable scaffolds fabricated by surface-selective laser sintering. Adv Mater **17,** 327, 2004.
39. Kuttenberger, J.J., and Hardt, N. Long-term results following reconstruction of craniofacial defects with titanium micro-mesh systems. J Maxillofac Surg **29,** 75, 2001.
40. Scholz, M., Eufinger, H., Wehmoller, M., Heuser, L., and Harders, A. CAD/CAM (computer-aided design/computer-aided manufacturing) titanium implants for cranial and craniofacial defect reconstruction. Zentralbl Neurochir **58,** 105, 1997.
41. Ho, S., Nallathamby, V., Ng, H., Ho, M., and Wong, M. A novel application of calcium phosphate-based bone cement

as an adjunct procedure in adult craniofacial reconstruction. Craniomaxillofac Trauma Reconstr **4,** 235, 2011.
42. Cohen, S.R., Holmes, R.E., Meltzer, H.S., Levy, M.L., and Beckett, M.Z. Craniofacial reconstruction with a fast resorbing polymer: a 6- to 12-month clinical follow-up review. Neurosurg Focus **16,** E12, 2004.
43. Hutmacher, D.W. Scaffolds in tissue engineering bone and cartilage. Biomaterials **21,** 2529, 2000.
44. Saiz, E., Zimmermann, E.A., Lee, J.S., Wegst, U.G., and Tomsia, A.P. Perspectives on the role of nanotechnology in bone tissue engineering. Dent Mater **29,** 103, 2013.
45. Dupont, K.M., Sharma, K., Stevens, H.Y., Boerckel, J.D., Garcia, A.J., and Guldberg, R.E. Human stem cell delivery for treatment of large segmental bone defects. Proc Natl Acad Sci U S A **107,** 3305, 2010.
46. Wozney, J.M., Rosen, V., Celeste, A.J., Mitsock, L.M., Whitters, M.J., Kriz, R.W., Hewick, R.M., and Wang, E.A. Novel regulators of bone formation: molecular clones and activities. Science **242,** 1528, 1988.
47. Riley, E.H., Lane, J.M., Urist, M.R., Lyons, K.M., and Lieberman, J.R. Bone morphogenetic protein-2: biology and applications. Clin Orthop Relat Res 39, 1996.
48. Ong, K.L., Villarraga, M.L., Lau, E., Carreon, L.Y., Kurtz, S.M., and Glassman, S.D. Off-label use of bone morphogenetic proteins in the United States using administrative data. Spine (Phila Pa 1976) **35,** 1794, 2010.
49. Chenard, K.E., Teven, C.M., He, T.C., and Reid, R.R. Bone morphogenetic proteins in craniofacial surgery: current techniques, clinical experiences, and the future of personalized stem cell therapy. J Biomed Biotechnol **2012,** 601549, 2012.
50. Park, J., Ries, J., Gelse, K., Kloss, F., von der Mark, K., Wiltfang, J., Neukam, F.W., and Schneider, H. Bone regeneration in critical size defects by cell-mediated BMP-2 gene transfer: a comparison of adenoviral vectors and liposomes. Gene Ther **10,** 1089, 2003.
51. Kaban, L.B., Glowacki, J., and Murray, J.E. Repair of experimental mandibular bony defects in rats. Surg Forum **30,** 519, 1979.
52. Schmitz, J.P., and Hollinger, J.O. The critical size defect as an experimental model for craniomandibulofacial nonunions. Clin Orthop Relat Res 299, 1986.
53. Higuchi, T., Kinoshita, A., Takahashi, K., Oda, S., and Ishikawa, I. Bone regeneration by recombinant human bone morphogenetic protein-2 in rat mandibular defects. An experimental model of defect filling. J Periodontol **70,** 1026, 1999.

Address correspondence to:
Pamela C. Yelick, PhD
Department of Orthodontics
Division of Craniofacial and Molecular Genetics
Tufts University School of Dental Medicine
Boston, MA 02111

E-mail: pamela.yelick@tufts.edu

Received: April 26, 2016
Accepted: June 28, 2016
Online Publication Date: July 13, 2016